

Effect of Number of Walls on Plasmon Behavior in Carbon Nanotubes

M. H. Upton,¹ R. F. Klie,¹ J. P. Hill,¹ T. Gog,² D. Casa,² W. K. Ku,¹
Y. Zhu,¹ M. Y. Sfeir,¹ J. M. Isenich,¹ G. Eres,³ and D. Lowndes³

¹Condensed Matter Physics and Materials Science Department,
Brookhaven National Laboratory, Upton, New York 11973

²CM C-XOR, Advanced Photon Source, Argonne National Laboratory, Argonne, Illinois 60439

³Condensed Matter Sciences Division, Oak Ridge National Laboratory, Oak Ridge, Tennessee 37830

Received: February 8, 2020

We investigate the physical parameters controlling the low energy screening in carbon nanotubes via electron energy loss spectroscopy and inelastic x-ray scattering. Two plasmon-like features are observed, one near 9 eV (the so-called plasmon) and one near 20 eV (the so-called + plasmon). At large nanotube diameters, the + plasmon energies depend exclusively on the number of walls and not on the radius or chiral vector. This shift indicates a change of strength of screening and the effective interaction at inter-atomic distance, and thus suggests an alternative mechanism of tuning the properties of the nanotube in addition to the well-known control provided by chirality and tube diameter.

PACS numbers: 73.22.-f, 73.20.Mf, 78.70.Ck

Carbon nanotubes (CNT) are perhaps the most promising, and most studied, mesoscopic system, in part because they have a wide range of interesting and unusual electronic properties. These include a long electron mean-free-path, quantized electronic and phonon bands and possible Tomonaga-Luttinger liquid behavior [1, 2, 3, 4, 5]. Much of this behavior arises because of the near one-dimensionality of the nanotubes which increases the importance of many-body effects in the system. The influence of many-body effects is controlled in part by the length scale of the low energy interactions. Determining which electronic properties depend on which physical parameters is one of the major goals of nanotube physics, as such control will lead to technological applications. For example, the binding energy of the exciton, important for solar energy applications, is influenced by the length scale of low energy interactions [6].

The three key physical parameters affecting the electronic properties of nanotubes are nanotube radius, chiral vector and number of walls: large curvatures in small-radius nanotube walls cause the and orbitals to hybridize; the chiral vector of nanotubes determines whether the nanotube is metallic or semiconducting; and finally, the number of walls and the nanotube radius both provide quantization conditions for the electron wave functions [1, 7]. However, it is not well understood what effect, if any, these parameters have on the length scale of low energy interactions. Because of the large influence of low energy interactions on the physics and possible applications of nanotubes, it is essential to investigate which parameters control their length-scale and strength. Electron energy loss spectroscopy (EELS) and inelastic x-ray scattering (IXS) are ideal tools for such an investigation, as they both directly probe the dielectric function which determines the screening of the bare interaction [8].

In this Letter, the plasmons of carbon nanotubes with a variety of different properties are studied and compared to those of bulk graphite. By taking advantage of the

complementary strengths of EELS and IXS it is possible to isolate the effects of three variables: diameter, chiral vector and number of walls, and determine that the plasmon frequencies vary only with the number of walls. The results imply that the low energy screening of nanotubes may be tuned simply by changing the number of walls.

We discuss first the measurement of the effect of the radius of the CNT (which changes the curvature of the walls). This was examined by performing low-loss EELS measurements of the plasmon energies. A number of EELS studies of plasmons in nanotubes have been previously performed [9, 10, 11, 12]. In particular, the plasmons of single nanotubes [11, 12] and of a randomly oriented, mainly single-walled CNT mat [10] have been studied. However, these studies did not examine the effects of nanotube diameter and number of walls separately. Further, these particular experiments often had limited resolution in reciprocal space and energy.

The present EELS measurements were performed on a number of isolated double-walled CNTs using an aberration corrected Scanning transmission electron microscope (JEOL JEM 2200FS), equipped with a Schottky field emission gun operated at 200 keV, an in-column omega energy filter and a CEOS probe corrector. The electron probe size (FWHM) was chosen to be 0.2 nm to provide sufficient electron beam intensity to study single nanotubes. The collection and convergence angles were 8.9 and 15 m rad respectively. The energy resolution was measured to be 1.0 eV. The beam spot was placed on the center of the tube so that the momentum transfer, which is perpendicular to the beam direction, was tangential to the walls of the nanotube.

The resulting energy loss spectra are shown in figure 1. These data in fact represent an integral over a disk in reciprocal space with a radius of $Q = 5.5 \text{ \AA}^{-1}$, because of the large acceptance of the detector and the beam convergence angle. Interpreting the spectra quantitatively is further complicated by multiple scattering effects, though

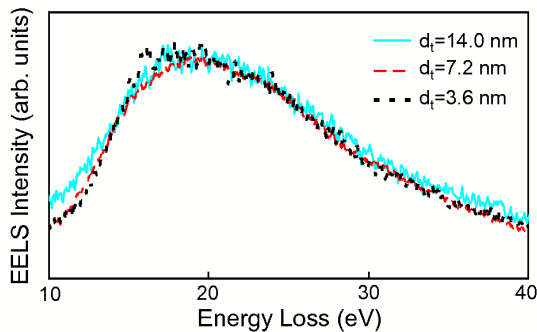


FIG. 1: (color online) EELs spectra from three double walled carbon nanotubes of different diameters. The blue, solid line is a spectrum from a double walled nanotube with a diameter of 14.0 nm ; the black, short-dashed line is from a double walled nanotube with a diameter of 7.2 nm and the red, long-dashed line is from a double walled nanotube with a diameter of 3.6 nm . The spectra are all taken at the same position in the Brillouin zone. The spectra have been normalized to the sample peak intensities and the elastic line has been subtracted of each one.

based on a comparison of the measured plasmon energies with the plasmon energy dispersions measured with IXS, discussed below, the EELs intensity appears to be dominated by contributions from close to $Q = 0$. For the purposes of the present study, however, the important point is that all EELs spectra are measured under identical conditions and therefore may be directly compared with each other.

Figure 1a shows measurements from three different, isolated, double-walled CNT with diameters of 3.6, 7.2 and 14.0 nm . These tubes were taken from the same aligned nanotube arrays discussed below. The + plasmon is clearly visible near 18 eV . Despite the drastically different diameters of the nanotubes, the + plasmon energies are identical. Although the chirality of the nanotubes was not explicitly checked it is impossible for nanotubes with different diameters to have the same chiral vectors. Further, it is less than 1% probable that even the two smallest nanotubes would have the same chiral angle. These results therefore explicitly demonstrate, for the first time, that the plasmon energy is independent of nanotube diameter and chirality, for large enough diameters.

As illustrated above, the great strength of EELs studies is their ability to study one nanotube at a time. Unfortunately, they suffer from limited momentum resolution and range. In particular, multiple scattering effects complicate the data analysis at large momentum transfers and one is restricted to looking at small momentum transfers. To address the momentum dependence of these features therefore, IXS is utilized.

IXS, like EELs, measures the dynamical structure fac-

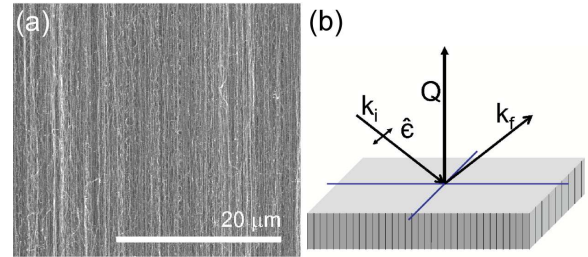


FIG. 2: (color online) (a) Scanning electron microscope picture of an aligned array of multi-walled carbon nanotubes and (b) schematic of the experimental geometry for the x-ray experiments. The axes of the nanotubes are parallel to the direction of momentum transfer, Q .

tor, $S(Q; \omega)$. The advantage of IXS is that the small x-ray scattering cross-section means that there are almost no multiple scattering inelastic events and the interpretation of the data is straightforward, even at high momentum transfers. However, IXS cannot look at individual nanotubes but requires an ensemble of nanotubes. The technique is described in detail elsewhere [8, 13]. The samples studied here were arrays of long, aligned carbon nanotubes [14]. These samples allow for a significant advance over earlier ensemble measurements because they allow measurements of nanotubes in one orientation, instead of an average of orientations. Thus the combination of IXS and aligned samples allow much more of reciprocal space to be probed than had been previously possible. We note that this is the first IXS study of carbon nanotubes, though there have been previous IXS studies of the plasmons of graphite [13, 15].

The aligned CNT samples studied here were grown on a Si(001) substrate by chemical vapor deposition [14]. Two types of samples were studied: aligned multi-walled and aligned few-walled carbon nanotube (MW- and FW-CNT) arrays. The tube axes are within 20 degrees of the substrate normal. A scanning electron microscope picture of one such MW CNT sample is shown in figure 2a. The nanotubes have a relatively low packing fraction (10% – 17%) and are not bunched in ropes, as verified by x-ray transmission and microprobe measurements. Therefore, because the nanotubes are too separated to strongly interact, we believe the results reported here are representative of individual nanotubes and not of a bundle of interacting nanotubes. This is an important point because the environment of a nanotube, for example, a substrate that a nanotube rests on, can change the properties of a nanotube [16, 17].

Quantitative measurements of the electronic properties of nanotube samples have no meaning without careful enumeration of the physical properties of the nanotubes. Therefore, the physical properties of these nanotube arrays have been characterized by a number of techniques including Raman spectroscopy, TEM and SAXS. In particular, a series of TEM images show that the MW CNT sample comprises tubes with an average outer diameter

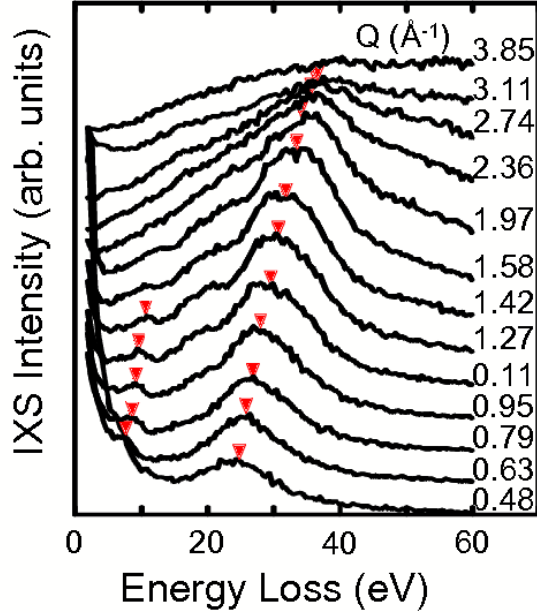


FIG. 3: (color online) Inelastic x-ray scattering spectra from the few-walled carbon nanotube sample shown in a stackplot. Q is parallel to the nanotubes' axis. The $+$ plasmon is the large feature between 20 and 40 eV energy loss. The plasmon is the small peak near 10 eV energy loss. The elastic lines have been omitted in these plots. A red triangle points to the peak positions.

of 19 6 nm and an average of 14 5 walls, while the nanotubes in the FWCNT sample have an average outer diameter of 5 2 nm and 3 2 walls. These parameters are consistent with the Raman measurements.

The IXS experiments reported here were performed at beam line 9-ID, CM C-XOR, at the Advanced Photon Source, Argonne National Laboratory. A Si(333) monochromator was used to monochromatize the incident photons and a spherically bent Ge(733) analyzer, with a radius of 1 m, focused the scattered radiation onto a solid-state detector. The overall resolution of this configuration was 300 meV (FWHM) and the beam size was 800 150 m². The incident photons were linearly polarized, perpendicular to the scattering plane, as shown in figure 2b. Energy loss scans were performed by varying the incident energy while holding the final energy fixed at 8.9805 keV. In all the data shown here, the direction of the momentum transfer was along the axes of the aligned nanotube samples. The samples are mounted with double sided tape on a copper block in a rough vacuum and visually aligned. Spectra were taken at room temperature. IXS spectra of the FWCNT sample are shown in figure 3 [18].

Both the $+$ and plasmon bands are visible in figure 3. The $+$ plasmon corresponds to the large peak seen near 30 eV and the plasmon corresponds to the smaller peak observed near 10 eV. To extract the plasmon peak

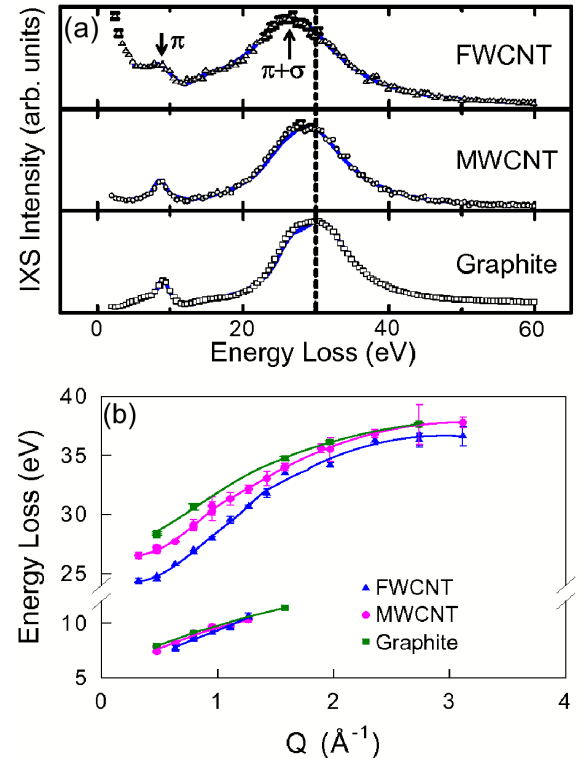


FIG. 4: (color online) (a) Inelastic x-ray scattering spectra from few-walled (top panel) and multi-walled carbon nanotube (middle panel) and HOPG (bottom panel). In each case, $Q = 0.79\text{ Å}^{-1}$ with Q along the nanotubes' axis and in the plane of graphite, respectively. The elastic lines have been omitted in this plot. (b) A complete plasmon dispersion for the three samples. The lines are a guide to the eye. The error bars come from the Marquardt least-squares fitting algorithm. When no error bars appear, the error is smaller than the symbol size.

positions, the spectra were fitted with Lorentzians. The quality of the fits to some of the data taken at intermediate momentum transfers was improved by fitting a low energy loss shoulder near 22 eV and a small amount of inter-band structure near 28 eV with additional Lorentzians [15]. Further, in the low momentum transfer MWCNT spectra (not shown), a Lorentzian was used to fit the low energy loss shoulder of the plasmon. The addition of these small Lorentzians does not affect the results of this paper, which focuses on the behavior of the large $+$ plasmon near 25 eV.

In figure 4a, representative inelastic spectra for the FWCNT, MWCNT and HOPG samples are shown. In each case, the data were taken at $Q = 0.79\text{ Å}^{-1}$. For nanotube samples, the momentum transfer was along the axes of the nanotubes and for the graphite sample the momentum transfer was in the plane of the graphite sheets. Note that the tail of the elastic line in the FWCNT spectrum appears unusually large simply because there is not much FWCNT material and the in-

elastic signal is therefore weak compared to that from the MW CNT and graphite samples; the MW CNT are 6 mm long while the FW CNT are only 2 mm long.

We note in passing that carbon nanotube properties are known to be sensitive to the surface adsorption of water and other atmospheric gases [19, 20, 21]. Surface adsorption effects were therefore looked for in these data by outgassing a sample in rough vacuum. Specifically, a sample was heated to 120 C over 90 minutes and then held at 120 C for 3 hours. There was no measurable difference between the observed plasmon energies before and after the outgassing procedure.

It is clear from figures 4a and b that the + plasmon energy is a function of the physical characteristics of the sample. At large Q , corresponding to small length scales, the difference between graphite, MW CNT and FW CNT

+ plasmon energies is small or nonexistent, indicating the inefficiency of screening at atomic length scales. At small and intermediate Q , corresponding to longer length scales, the differences in the plasmon energies are significant, with samples with fewer walls exhibiting a significantly lower plasmon energy than those with more walls. The energy difference is noticeable for $Q = 2 \text{ \AA}^{-1}$, corresponding to lengths greater than 3 Å, near the interplanar distance in graphite. The plasmon energy is determined by the zero of the energy and wave-vector dependent dielectric function, (Q) . From a general understanding of the dielectric constant, we see that this implies that, at low energies, the magnitude of the dielectric function is smaller in samples with fewer walls. This indicates that the length scale of low energy interactions

is longer in FW CNT than in MW CNT, and longer in MW CNT than in graphite. There are a number of consequences of changes in this length scale for the optical properties of the system. For example, it implies that excitons in MW CNT are more likely to dissociate than excitons in FW CNT, because the additional screening in MW CNT decreases the binding energy of excitons.

In summary, we have shown that for diameters larger than 3.6 nm, the plasmon energies near $Q = 0$ of CNT samples depend exclusively on the number of walls. That is, a unique plasmon dispersion and a unique + plasmon energy at $Q = 0$ are associated with a particular number of walls. This energy shift implies that the low energy screening, which controls the physical extent of the low energy interactions, can be tuned by changing the number of walls in carbon nanotubes.

The authors thank C. C. Homes and L. Carr for optical characterization of the samples and A. Stein for electron microprobe pictures of the samples. Work performed at BNL was supported by US DOE, Division of Materials Science and Engineering, under contract No. DE-AC 02-98CH 10886 and partially by DOE-CMNS. Use of the Advanced Photon Source was supported by the US DOE, Office of Science, Office of Basic Energy Sciences, under Contract No. W-31-109-Eng-38. Research performed at ORNL was sponsored by the Division of Materials Sciences and Engineering, Office of Basic Energy Sciences, US DOE, under contract DE-AC 05-000 R 22725 with Oak Ridge National Laboratory, managed and operated by UT-Battelle, LLC.

[1] R. Saito, G. D. Dresselhaus, and M. S. Dresselhaus, *Physical Properties of Carbon Nanotubes* (Imperial College Press, 1998).

[2] J. Hone, B. Batlogg, Z. Benes, A. T. Johnson, and J. E. Fischer, *Science* 289, 1730 (2000).

[3] B. Gao, A. Komnik, R. Egger, D. C. G. Lattli, and A. Bachthold, *Phys. Rev. Lett.* 92, 216804 (2004).

[4] R. Tarkiainen, M. A. Halskog, J. Penttila, L. Roschier, P. Hakonen, M. Paalanen, and E. Sonin, *Phys. Rev. B* 64, 195412 (2001).

[5] M. Bockrath, D. H. Cobden, J. Lu, A. G. Rinzler, R. E. Smalley, L. Balents, and P. L. McEuen, *Nature* 397, 598 (1999).

[6] V. Perebeinos, J. Terso, and P. Avouris, *Phys. Rev. Lett.* 92, 257402 (2004).

[7] M. Y. Sfeir, T. Beetz, F. Wang, L. Huang, X. M. H. Huang, M. H. Huang, J. Hone, S. O'Brien, J. A. M. Isweich, T. F. Heinz, et al., *Science* 312, 554 (2006).

[8] W. Schulke, *Handbook on Synchrotron Radiation* (Elsevier Science Publishers B.V., 1991), vol. 3, chap. 15, pp. 565-638.

[9] T. Pichler, M. Knapfer, M. S. Golden, J. Fink, A. Rinzler, and R. E. Smalley, *Phys. Rev. Lett.* 80, 4729 (1998).

[10] M. Kociak, L. Henrad, O. Stephan, K. Suenaga, and C. Colliex, *Phys. Rev. B* 61, 13936 (2000).

[11] L. A. Bursill, P. A. Stadelmann, J. L. Peng, and S. Prater, *Phys. Rev. B* 49, 2882 (1994).

[12] P. M. A. Jayan, S. Iijima, and T. Ichihashi, *Phys. Rev. B* 47, 6859 (1993).

[13] W. Schulke, U. Bonse, H. N. Agasawa, A. Kaprolat, and A. Berthold, *Phys. Rev. B* 38, 2112 (1988).

[14] G. Eres, A. A. Puretzky, D. B. G. Eohegan, and H. Cui, *Appl. Phys. Lett.* 84, 1759 (2004).

[15] N. Hiraoka, H. Ishii, I. Jarrige, and Y. Q. Cai, *Phys. Rev. B* 72, 075103 (2005).

[16] B. J. LeRoy, S. G. Lemay, J. K. Ong, and C. D. Eckler, *Appl. Phys. Lett.* 84, 4280 (2004).

[17] A. G. M. Marinopoulos, L. Reining, A. Rubio, and V. Otero, *Phys. Rev. B* 69, 245419 (2004).

[18] The spectra are normalized by incident x-ray intensity and a geometric factor, $1 - \cos \theta$, which accounts for variations in the beam footprint on the sample as the scattering angle is varied.

[19] A. Zahab, L. Spina, P. Poncharal, and C. M. Ariére, *Phys. Rev. B* 62, 10000 (2000).

[20] P. G. Collins, K. Bradley, M. Ishigami, and A. Zettl, *Science* 287, 1801 (2000).

[21] J. Kong, N. R. Franklin, C. Zhou, M. G. Chapline, S. Peng, K. Cho, and H. Dai, *Science* 287, 622 (2000).